The ^{31}P NMR Chemical Shielding Tensors in Quaternary Metal Thiophosphates, $NaNb_2PS_{10}$, $AgNb_2PS_{10}$, $Au_{0.5}Nb_2PS_{10}$, and $NaSmP_2S_6$

Ae Ja Woo,* Sung-Jin Kim, Young Sun Park, and Eun-Young Goh

Department of Science Education and Department of Chemistry, Ewha Womans University, Seoul 120-750, Korea

Received January 22, 2001. Revised Manuscript Received October 10, 2001

For quaternary metal thiophosphates, $NaNb_2PS_{10}$, $AgNb_2PS_{10}$, $Au_{0.5}Nb_2PS_{10}$, and $NaSmP_2S_6$, the principal elements of the ^{31}P NMR chemical shielding tensor (δ_{11}, δ_{22}, and δ_{33}) are acquired from the nonlinear least-squares fitting the static powder patterns and MAS spectra. Isotropic chemical shift (δ_{iso}) and chemical shielding anisotropy ($\Delta\delta$) have been employed to correlate with the X-ray crystallographic data, the average (P−S) bond length and the average (S−P−S) bond angle deviation from 109.5°, respectively, at the tetrahedrally coordinated phosphorus atoms. On the basis of these successful correlations, the charge transfer from Na, Ag, and Au metals to the (P−S) ligand is discussed and complemented by the band-structure calculation.

Introduction

Transition-metal thiophosphates have been actively investigated because of their potential importance as host materials for secondary lithium batteries, nonlinear optics, and ion-exchange applications.[1] Useful properties for the applications are due to their structural low dimensionality, and current research interest in this area is focused on the host capacity of host materials and their electronic modifications induced by guest species. Well-known examples of low-dimensional transition-metal thiophosphates include MPS_3 (M = Mn, Fe, Cd, Co, Ni, and Zn),[2] V_2PS_{10},[3] Nb_2PS_{10},[4] $Nb_4P_2S_{21}$,[5] and NbP_2S_8.[6] Previous band-structure investigation on layered ternary thiophosphates suggests that the empty or partially filled d-block orbitals of transition metals are responsible for lithium intercalation to Nb_2PS_{10}.[7] On the other hand, solid-state ^{31}P NMR work implies that electrons from alkali metal K are transferred to p-orbitals of P rather than d-orbitals of Nb in Nb_2PS_{10}.[8] Since not many examples of alkali metal intercalated thiophosphates with stable structures are structurally characterized, the effects of bonding and electronic structural change upon alkali metal cation intercalation have not been completely understood.

Recently, the metal intercalated thiophosphates ANb_2PS_{10} (A = Na, Ag, and Au)[9,10] and $NaSmP_2S_6$[9a] have been synthesized and have provided more information about the reduction centers in this family of compounds. Although the structure of $NaSmP_2S_6$ is not an isostructure of ANb_2PS_{10}, we include $NaSmP_2S_6$ in this investigation because not many cation intercalated thiophosphates with known crystal structures have been reported. The structures of ANb_2PS_{10} consist of one-dimensional infinite chains built by $[Nb_2S_{12}]$ and $[PS_4]$ units. The Nb atoms are centered in distorted bicapped trigonal prismatic polyhedra, and neighboring polyhedra share square faces and edges to make Nb−Nb pairs. Tetrahedral $[PS_4]$ units are composed of one S atom at the prism corner and two other capping S atoms and an additional terminal S atom. Ag^+ and Na^+ cations in $AgNb_2PS_{10}$ and $NaNb_2PS_{10}$ reside in exactly the same site in the van der Waals gap between infinite chains; however, Au atoms in $Au_{0.5}Nb_2PS_{10}$ are in slightly different sites and partially occupied. $NaSmP_2S_6$ is one of the derivatives of the $M^IM^{III}P_2S_6$ (M^I = monovalent cation and M^{III} = trivalent cation) family, where MPS_3-type layers are condensed together. MPS_3-type layers consist of M^{2+} cation coordinated to ethane-like $P_2S_6^{4-}$ bridging ligands. In Figure 1a and b, the crystal

* To whom correspondence should be addressed. E-mail: ajwoo@mm.ewha.ac.kr.

(1) (a) Brec, R.; Schleigh, D.; Louisy, A.; Rouxel, J. *Ann. Chim. Fr.* **1978**, *3*, 347. (b) Barj, M.; Sourisseau, C.; Ouvrard, G.; Brec, R. *Solid State Ionics* **1983**, *11*, 179. (c) Brec, R.; Schleigh, D.; Louisy, A.; Rouxel, J. *Inorg. Chem.* **1979**, *18*, 1814. (d) Barj, M.; Sourisseau, C.; Ouvrard, G.; Brec, R. *Solid State Ionics* **1983**, *11*, 179. (e) Lacroix, P. G.; Clement, R.; Nakatani, K.; Zyss, J.; Ledoux, L. *Science* **1994**, *263*, 658. (f) Lagadic, I.; Lacroix, P. G.; Clement, R. *Chem. Mater.* **1997**, *9*, 2004. (g) Clement, R. *J. Chem. Soc., Chem. Commun.* **1980**, 647. (h) Michalowicz, A.; Clement, R. *Inorg. Chem.* **1982**, *21*, 3892.

(2) (a) Ouvrard, G.; Brec, R.; Rouxel, J. *Mater. Res. Bull.* **1985**, *20*, 1181. (b) Brec, R.; Ouvrard, G.; Rouxel, J. *Mater. Res. Bull.* **1985**, *20*, 1257. (c) Prouzet, E.; Ouvrard, G.; Brec, R. *Mater. Res. Bull.* **1986**, *21*, 195.

(3) Brec, R.; Ouvrard, G.; Evain, M.; Grenouilleau, P.; Rouxel, J. *J. Solid State Chem.* **1983**, *7*, 174.

(4) Brec, R.; Grenouilleau, P.; Evain, M.; Rouxel, J. *Rev. Chim. Miner.* **1983**, *20*, 295.

(5) Brec, R.; Evain, M.; Grenouilleau, P.; Rouxel, J. *Rev. Chim. Miner.* **1983**, *20*, 283.

(6) Grenouilleau, P.; Brec, R.; Evain, M.; Rouxel, J. *Rev. Chim. Miner.* **1983**, *20*, 628.

(7) Evan, M.; Brec, R.; Whangbo, M.-H. *J. Solid State Chem.* **1987**, *71*, 244.

(8) Han, O. H.; Yun, H.-S. *Bull. Korean Chem. Soc.* **2000**, *21*, 671.

(9) (a) Goh, E.-Y.; Kim, S.-J. *Synthesis and Crystal Structure of New Quaternary Thiophosphates.* M.S. Thesis, Ewha Womans University, 2000. (b) Goh, E.-Y.; Kim, E.-J.; Kim, S.-J. *J. Solid State Chem.* **2001**, *159*, 195−204.

(10) Do, J.-H.; Yun, H.-S. *Inorg. Chem.* **1996**, *35*, 3729.

10.1021/cm010053v CCC: $22.00
Published on Web 01/11/2002

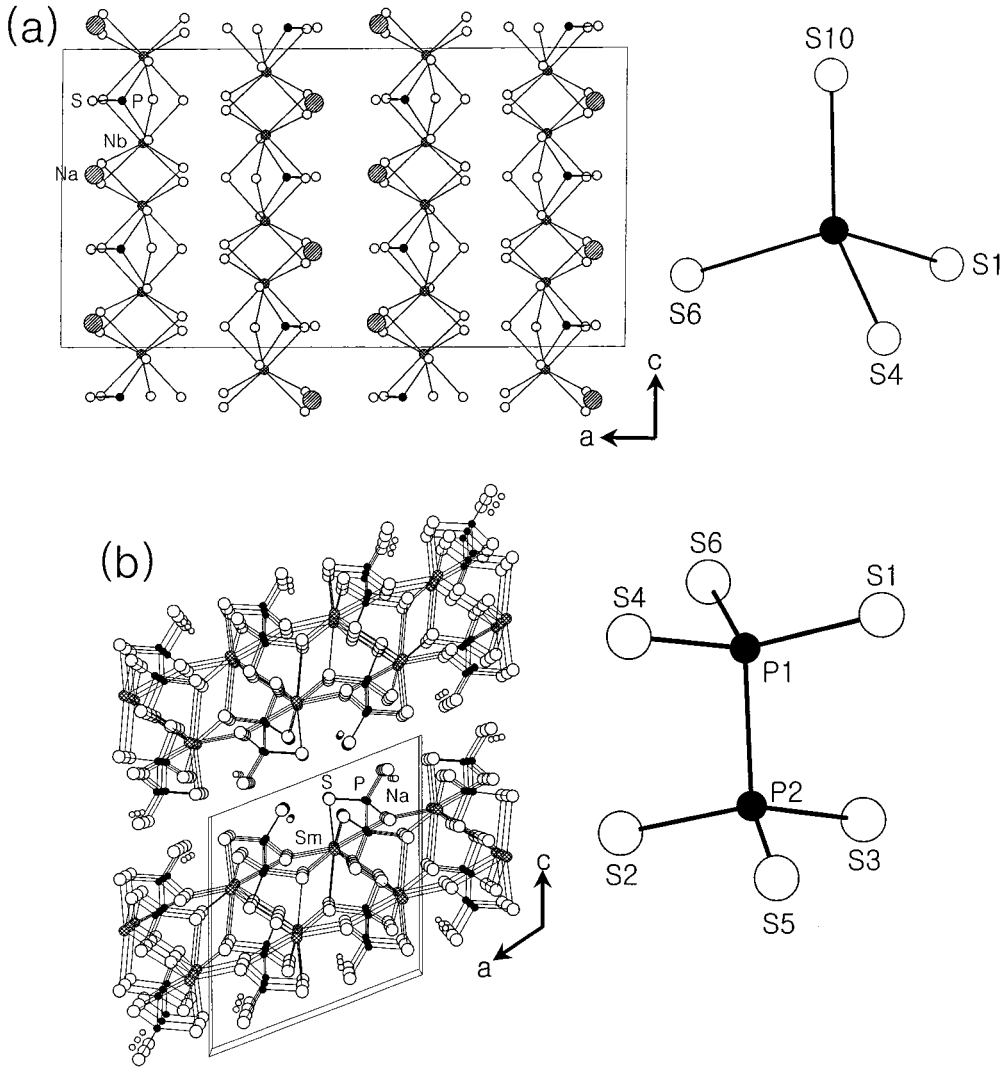

Figure 1. Crystal structures of (a) $NaNb_2PS_{10}$ and (b) $NaSmP_2S_6$ projected along the *b*-axis. The unit cell boundaries are shown. Local structures around P atoms in the tetrahedral PS_4^{3-} unit of $NaNb_2PS_{10}$ and in the ethane-like $P_2S_6^{4-}$ unit of $NaSmP_2S_6$ are also shown.

structures of $NaNb_2PS_{10}$ and $NaSmP_2S_6$ are shown, respectively, projected along the *b*-axis. Local structures around P atoms in the tetrahedral PS_4^{3-} unit of $NaNb_2PS_{10}$ and in the ethane-like $P_2S_6^{4-}$ unit of $NaSmP_2S_6$ are also shown.

Herein, we are trying to obtain information on electron transfers from intercalated metals to Nb_2PS_{10} and the SmP_2S_6 parts in $NaNb_2PS_{10}$, $AgNb_2PS_{10}$, and $Au_{0.5}Nb_2PS_{10}$ and $NaSmP_2S_6$, respectively, by using solid-state ^{31}P NMR spectroscopy. The relationships between the ^{31}P NMR isotropic chemical shift and the average (P−S) bond length and between the ^{31}P NMR chemical shielding anisotropy and the deviation of (S−P−S) bond angle from the ideal tetrahedral are described. In addition, the solid-state NMR results are compared with the results of band-structure calculation.

Experimental Section

Sample Preparation. $NaNb_2PS_{10}$ was made by the mixture of Na_2S (Kojundo, 99%), Nb (Kojundo, 99.9%), P_2S_5 (Fluka, >98%), and S (Aldrich, 99.999%) powders in stoichiometric ratio. $AgNb_2PS_{10}$ and $Au_{0.5}Nb_2PS_{10}$ were prepared from the stoichiometric amount of mixture of Ag (Kojima, 99.99%), Au (Mi Kueong Sa, 99.99%), Nb, P, and S powders. $NaSmP_2S_6$ was prepared from the mixture of Na_2S, Sm (Aldrich, 99.9%), P (Aldrich, 99.99%), and S powders in stoichiometric ratio. The reaction mixtures were doubly sealed in evacuated quartz tubes and heated at 900 °C for five days. The detailed procedures are described in a later reference.[9]

Electronic Structure Calculation. Electronic-structure calculations were performed by the extended Hückel method within the framework of the tight-binding approximation.[11] Density of states (DOS) and crystal orbital overlap populations (COOP) were calculated on the basis of given crystal structure. The atomic orbital parameters employed in the calculation were default values in the CAESAR program, which are listed in Table 1.

Solid-State ^{31}P NMR Spectroscopy. Solid-state ^{31}P NMR static powder patterns and MAS (Magic Angle Spinning) spectra were taken at 81.077 and 161.982 MHz on a Varian UnityInova200 and a Bruker DSX400 solid-state NMR spectrometer, respectively. The spectra were acquired as a single pulse or spin−echo following a 20 μs delay, and a CP/MAS high-power probe with a solenoidal coil was used. At 81.077 MHz resonance frequency, the 90° pulse length used for excitation was 5.5 μs. At 161.982 MHz, 90° pulse of 2.4 μs was used. A relaxation delay of 1 s was used. Typically, ~200 and

(11) (a) Hoffman, R. *J. Chem. Phys.* **1963**, *39*, 1397. (b) Ren, J.; Liang, W.; Whangbo, M.-H. CAESAR; Primecolor Software, Inc.: Cary, NC, 1999.

Table 1. Atomic Orbital Parameters Used in Extended Hückel Calculations

atom	orbital	H_{ii} (eV)[a]	ζ_1	C_1	ζ_2	C_2
S	3s	−20.0	2.122	1.0		
S	3p	−13.3	1.827	1.0		
P	3s	−18.6	1.75	1.0		
P	3p	−14.0	1.30	1.0		
Nb	5s	−10.1	1.89	1.0		
	5p	−6.86	1.85	1.0		
	4d	−12.1	4.08	0.6401	1.64	0.5516

[a] $H_{ii} = \langle\chi_i|H^{eff}|\chi_i\rangle$, $i = 1, 2, 3,....$ The value approximated by valence-state ionization potential.

~1000 free induction decays for static powder patterns and MAS spectra, respectively, were acquired. ^{31}P NMR chemical shifts on the δ-scale are referenced through an external 85% aqueous solution of H_3PO_4 at 0 ppm.

The relative assignment of the principal elements of the ^{31}P NMR chemical shielding tensor is $\delta_{11} \geq \delta_{22} \geq \delta_{33}$ with an isotropic chemical shift $\delta_{iso} = (\delta_{11} + \delta_{22} + \delta_{33})/3$. Chemical shielding anisotropy ($\Delta\delta$) is derived from the following equations;[12]

$$\Delta\delta = (3/2)(\delta_{11} - \delta_{iso}) \text{ for } |\delta_{11} - \delta_{iso}| \geq |\delta_{33} - \delta_{iso}|$$

and

$$\Delta\delta = (3/2)(\delta_{33} - \delta_{iso}) \text{ for } |\delta_{33} - \delta_{iso}| \geq |\delta_{11} - \delta_{iso}|$$

Results and Discussion

Figure 2a and c shows experimental ^{31}P NMR static powder pattern and MAS spectrum acquired at 81.077 MHz resonance frequency, respectively, for $AgNb_2PS_{10}$. The center band showing an isotropic chemical shift at 122.8 ppm is marked by the asterisk (*). The very small peak around 0 ppm is considered as an impurity represented by a cross (†). Figure 2b shows the best calculated fit to the static powder pattern. The powder pattern is calculated by solving the time-independent Hamiltonian because of the chemical shielding interaction. The line intensities of the central and spinning sidebands are calculated by using the Herzfeld−Berger method.[13] To confirm the chemical shielding tensor elements determined from the powder pattern, a stick plot to the line intensities of MAS spectrum shown in Figure 2d was calculated with the same values as used for the simulation of the powder pattern. The ^{31}P NMR static and MAS patterns (not shown here) obtained for $NaNb_2PS_{10}$ are very similar to those for $AgNb_2PS_{10}$. Shown in Figure 3a and b are the experimental ^{31}P NMR powder pattern and the MAS spectrum acquired at 161.982 MHz for $Au_{0.5}Nb_2PS_{10}$. Figure 3c is the best calculated stick plot to the line intensities in the MAS spectrum. The ^{31}P NMR powder pattern in $Au_{0.5}Nb_2PS_{10}$ shows an inhomogeneously broadened line shape, so it is not easy to extract the NMR chemical shielding parameters without loss of accuracy. Figure 4a and b are experimental ^{31}P NMR static powder patterns taken with spin−echo pulse at 161.982 MHz and with single pulse at 81.077 MHz, respectively, for $NaSmP_2S_6$. ^{31}P MAS spectrum in Figure 4d clearly shows that $NaSmP_2S_6$ has two magnetically inequivalent P sites, P1 and P2, whose isotropic chemical shifts are 91.1 and 121.7 ppm, respectively. Figure 4c shows the best calculated

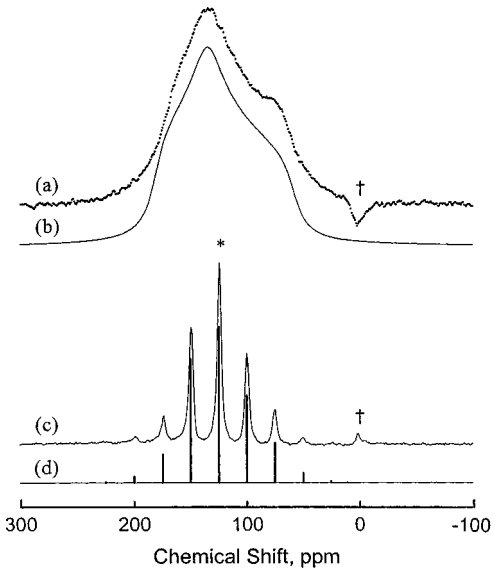

Figure 2. (a) Experimental ^{31}P NMR static powder pattern (···), (b) the best calculated fit to the powder pattern (—), (c) experimental MAS spectrum (—) at a spinning rate of 2.2 kHz, and (d) the stick plot to the MAS spectrum (—) calculated by using the same chemical shielding values as in (b) for $AgNb_2PS_{10}$. All spectra were obtained at 81.077 MHz resonance frequency. Isotropic chemical shift is marked by an asterisk (*). Peak (†) at 0 ppm indicates an impurity.

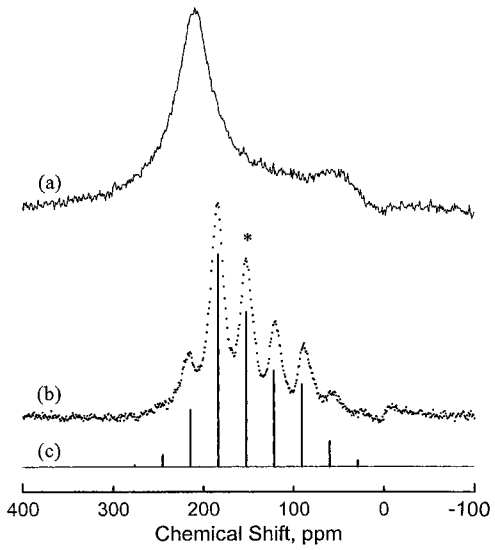

Figure 3. (a) Experimental ^{31}P NMR static powder pattern (—), (b) MAS spectrum (···) at a spinning rate of 5.0 kHz, and (c) the best calculated stick plot (—) to the MAS spectrum for $Au_{0.5}Nb_2PS_{10}$. All spectra were obtained at 161.982 MHz resonance frequency.

fit to the static powder pattern composed of two components from P1 and P2 sites in $NaSmP_2S_6$. The powder patterns in Figure 4a and b show exactly the same line shapes regardless of the applied magnetic field strengths. Thus, the homonuclear dipolar interaction between (P−P) bond in the ethane-like $P_2S_6^{4-}$ unit is negligible, and the spectral calculation is based on the only chemical shielding interaction.

The nonlinear least-squares fitting method using a Levenberg−Marquardt algorithm[14] was used to extract

(12) Duncan, T. M. *A Complication of Chemical Shift Anisotropies*; The Farragut Press: Chicago, 1990.

(13) Herzfeld, J.; Berger, A. E. *J. Chem. Phys.* **1980**, *73*, 6021.

(14) Kim, A. J.; Butler, L. G. *Concepts Magn. Reson.* **1992**, *4*, 205.

Table 2. ^{31}P NMR Chemical Shielding Parameters (ppm) and X-ray Crystallographic Bond Distances (Å) and Bond Angle Deviations from 109.5 (°)

							$NaSmP_2S_6$	
	$AgNb_2PS_{10}$	$Au_{0.5}Nb_2PS_{10}$	KNb_2PS_{10}[8]	$NaNb_2PS_{10}$	Nb_2PS_{10}[4,8]	$Nb_4P_2S_{21}$[5]	P1	P2
δ_{11}	181.2(2)	223.3(8)	177.5	183.7(1)	182.0		135.8(6)	168.2(5)
δ_{22}	133.1(2)	178.4(8)	133.5	134.4(1)	118.0		123.3(6)	132.6(6)
δ_{33}	54.1(4)	54.6(11)	39.5	46.4(3)	77.0		14.2(9)	64.3(8)
δ_{iso}	122.8(3)	152.1(3)	116.8	121.5(3)	125.7		91.1(3)	121.7(3)
$\Delta\delta$	103.1(5)	146.3(11)	116.0	112.6(4)	84.5		115.4(9)	86.1(8)
d(P−S)	2.039(5)	2.040(3)	2.036(5)	2.039(3)	2.052(4)	2.049(5)	2.007(5)	2.027(5)
Δ(∠S−P−S)	4.6(1)	4.3(5)	4.9(2)	4.6(2)	3.5(2)	3.4(5)	5.4(2)	3.7(2)
d(Nb−S)	2.542(3)	2.538(2)	2.541(4)	2.550(2)	2.547(4)	2.552(4)		

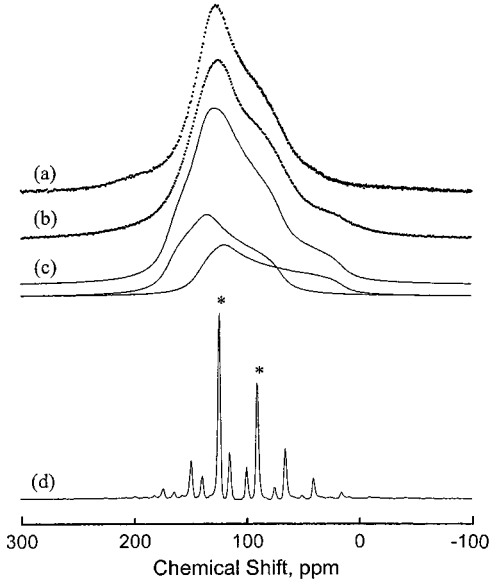

Figure 4. (a) and (b) Experimental ^{31}P NMR static powder patterns (···) acquired at 161.982 and 81.077 MHz, respectively, (c) the best calculated fit to the powder pattern and its two components (—), and (d) experimental MAS spectrum (—) at a spinning rate of 2.2 kHz at 81.077 MHz for $NaSmP_2S_6$. There are two sets of spinning sidebands, and their isotropic chemical shifts are represented by asterisks (*).

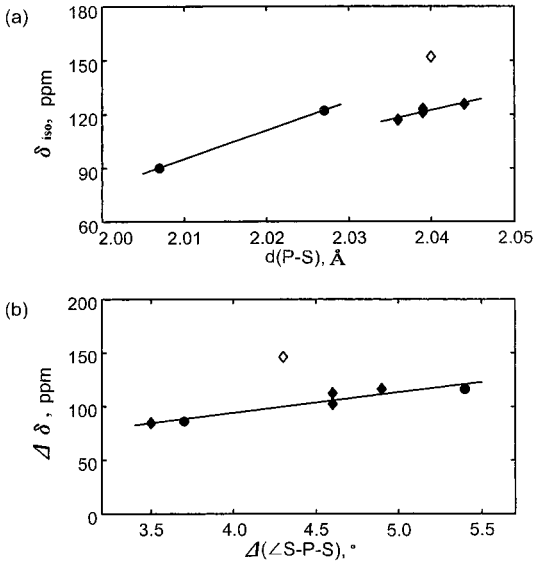

Figure 5. (a) Plot of ^{31}P NMR isotropic chemical shift (δ_{iso}) vs average (P−S) bond length (d(P−S)) at the tetrahedral P sites. (b) Plot of ^{31}P NMR chemical shielding anisotropy ($\Delta\delta$) vs average deviation of (S−P−S) bond angle from 109.5°(Δ-(∠S−P−S)). The data represented as circles (●) and diamonds (◆) were obtained from the ethane-like $P_2S_6^{4-}$ unit in $NaSmP_2S_6$ and the tetrahedral PS_4^{3-} unit in $NaNb_2PS_{10}$, $AgNb_2PS_{10}$, Nb_2PS_{10}, and KNb_2PS_{10}, respectively. The large deviated data points (◇) from $Au_{0.5}Nb_2PS_{10}$ were not included in the fittings.

the NMR chemical shielding parameters. The fitted variables include δ_{11} and δ_{22}; the value of δ_{33} is determined from δ_{11}, δ_{22}, and δ_{iso} obtained from the central band of the MAS spectrum. The principal elements of the ^{31}P NMR chemical shielding tensors (δ_{11}, δ_{22}, and δ_{33}) and the isotropic chemical shifts (δ_{iso}) and chemical shielding anisotropies ($\Delta\delta$) for our $NaNb_2PS_{10}$, $AgNb_2PS_{10}$, $Au_{0.5}Nb_2PS_{10}$, and $NaSmP_2S_6$ as well as for previously reported[8] Nb_2PS_{10} and KNb_2PS_{10} are listed in Table 2. Crystallographic bond distances and bond angles are the values reported previously from single-crystal X-ray diffraction experiments.[9] Only crystallographic data of $Nb_4P_2S_{21}$,[5] which has a similar structure to Nb_2PS_{10}, are also listed for comparison.

Shown in Figure 5a is a linear correlation between the ^{31}P NMR isotropic chemical shift and the average bond length of (P−S) bonds of the tetrahedrally coordinated P atom. Also, the linear correlation between the ^{31}P NMR chemical shielding anisotropy and the average deviation of (S−P−S) bond angle from 109.5° is established in Figure 5b. The data represented as diamonds (◆) and circles (●) were obtained from PS_4^{3-} units in ANb_2PS_{10} except $Au_{0.5}Nb_2PS_{10}$ and from $P_2S_6^{4-}$ units in $NaSmP_2S_6$, respectively. The relationships between the ^{31}P NMR chemical shielding and the X-ray crystallographic structural data are already well known for orthophosphate compounds composed of PO_4 units.[15,16] The large deviated data points (◇) from $Au_{0.5}Nb_2PS_{10}$ were not included in the fittings. The deviations may occur by the electron density irregularity around P atoms because of the partially occupied Au sites. It could be understood by the fact that the solid-state NMR spectra are represented by summing transition frequencies over all possible structures, while X-ray crystallographic data were obtained from the average atomic positions over the long-range ordered crystal.

The ^{31}P NMR isotropic chemical shift on the δ-scale moves downfield as the (P−S) bond length becomes longer, which corresponds to less shielding in the ^{31}P nucleus. We can explain an important feature on the basis of this relationship; it is possible to compare the nature of the chemical bondings in Nb_2PS_{10}, $NaNb_2PS_{10}$, KNb_2PS_{10}, and $AgNb_2PS_{10}$. According to the ^{31}P NMR isotropic chemical shifts, the electrons from K, Na, and Ag metals seem to transfer to the Nb_2PS_{10} part and

(15) Turner, G. L.; Smith, K. A.; Kirkpatrick, R. J.; Oldfield, E. *J. Magn. Reson.* **1986**, *70*, 408.
(16) Andrew, E. R.; Bryant, D. J.; Cashell, E. M.; Dunell, B. A. *Chem. Phys. Lett.* **1981**, *77*, 614.

occupy the (P−S) orbitals. If there is a significant amount of electron transfer from cation to (P−S) bonds, the (P−S) distance should decrease because of its bonding character as described in the band-calculation part. As shown in Table 2, all of the (P−S) distances in ANb_2PS_{10}, regardless of size or electronegativity of cations, are shorter than those in Nb_2PS_{10} and $Nb_4P_2S_{21}$. The shorter (P−S) bond lengths in intercalated ANb_2PS_{10} are an indication of electron transfer from cation. The crystallographic fact that intercalated monovalent cations are located near the S atoms of the PS_4^{3-} unit supports the possibility of electron transfer into the PS_4^{3-} unit. In addition, although both the $P_2S_6^{4-}$ and PS_4^{3-} units have the tetrahetrally coordinated P atom, the correlation between the ^{31}P NMR isotropic chemical shift and the average (P−S) bond length in the ethane-like $P_2S_6^{4-}$ unit for $NaSmP_2S_6$ is very close but not exactly consistent with that in the tetrahedral PS_4^{3-} unit in ANb_2PS_{10}. However, we can suggest that the P1 site is located closer to the Na atom than the P2 site in $NaSmP_2S_6$, which is consistent with the X-ray crystallographic data.[9] It might also be explained by the above-described result that the electropositive Na metal donates electrons to the ligand (P−S) bonding orbitals, the bond length becomes shorter, and consequently the ^{31}P chemical shielding becomes larger.

There is no notable feature in the (Nb−S) bond lengths of the six compounds. For example, since the electron donating ability of a K atom is greater than a Na atom, (Nb−S) bond lengths in KNb_2PS_{10} are expected to be longer than those of $NaNb_2PS_{10}$. However, it does not suggest that the assumption of electron transfer from cation to (Nb−S) bond is not correct. These conclusions do not agree with that obtained from the tight-binding band calculation for Li intercalated Nb_2PS_{10}. Whangbo et al.[7] suggested that the low-lying acceptor orbitals responsible for lithium intercalation of thiophosphates are d-block bands of Nb atoms. Since there are some structural changes in our cation intercalated thiophosphates, the rigid structural model of ternary compounds assuming only electron transfer within the intact structure is not applicable.

Figure 6a and b shows the DOS (Density Of State) and COOP (Crystal Orbital Overlap Population) curves obtained by the band-structure calculation for $(Nb_2PS_{10})^{1-}$ framework of $NaNb_2PS_{10}$. The DOS plot contains the total densities together with projections for the d-block states of Nb and p-block states of S and P atoms. Since the Fermi level cuts the top of the valence states, the DOS plot indicates that this material is a semiconductor. The top of the valence states consists of d-block states of Nb, and p-block states of S and P atoms are mixed as shown in projections of the DOS plot. The conduction band consists of d-block levels of Nb atoms, where p-block states of S and P atoms are mixed. The COOP plot shows that the overlap populations for (Nb−S) contacts are negative near the Fermi level indicating a strongly antibonding character on (Nb−S) interaction. However, the overlap populations for (P−S) contacts indicate a bonding interaction. Therefore, the results of band calculation suggest that the electrons from A cations in ANb_2PS_{10} are likely accommodated in (P−S) bonding orbitals rather than (Nb−S) antibonding orbitals.

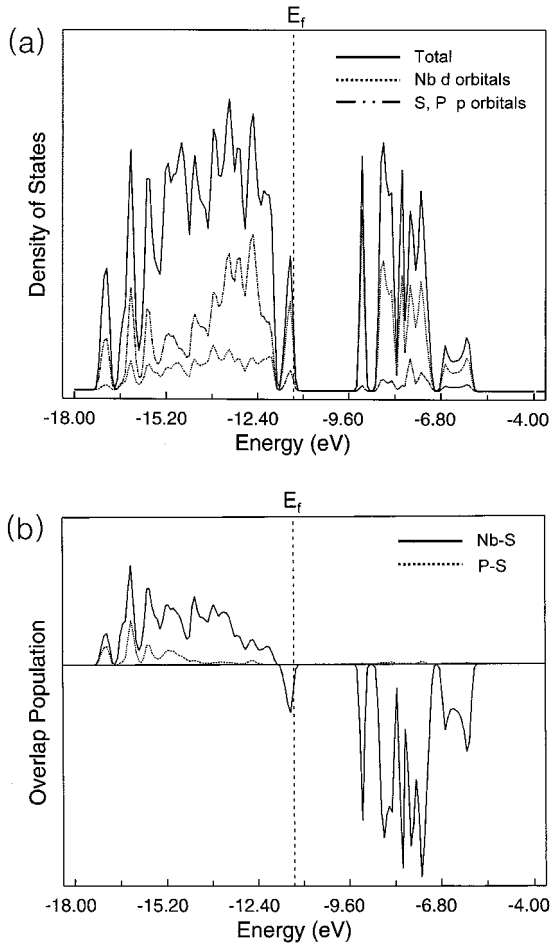

Figure 6. (a) DOS and projected DOS curves for $NaNb_2PS_{10}$. The projections of d-block band of Nb (···), p-block band of P and S atoms (—··), and total DOS (—) curves are shown. (b) COOP curves of Nb−S (—) and P−S (···) interaction for $NaNb_2PS_{10}$.

From the evidence found in the band calculation as well as in the solid-state NMR experiment, we can explain the local symmetry distortion in PS_4^{3-} units upon the intercalation of the Na, K, and Ag metals to Nb_2PS_{10}. Herein, it is not possible to determine the orientation of the principal elements of the ^{31}P NMR chemical shielding tensor relative to the molecular axis system in the PS_4^{3-} unit. However, we can expect that the δ_{33} axis may orient near the shortest (P−S) bond axis though, since δ_{33} is the smallest value of the three principal elements. The smallest δ_{33} in the five compounds is shown in KNb_2PS_{10} because the K metal is the most electropositive (vide ante). Consequently, as the electropositivity of the metal increases, the ^{31}P NMR chemical shielding anisotropy becomes larger, which is consistent with the average (S−P−S) bond angle deviation from 109.5°.

Conclusions

In the quaternary metal thiophosphates, $NaNb_2PS_{10}$, $AgNb_2PS_{10}$, and $NaSmP_2S_6$ including Nb_2PS_{10} and KNb_2PS_{10},[8] the ^{31}P NMR isotropic chemical shift (δ_{iso}) and the ^{31}P chemical shift anisotropy ($\Delta\delta$) are sensitive to the (P−S) bond length and the deviation of (S−P−S)

bond angle from 109.5°, respectively. On the basis of these NMR results, we conclude that electron transfers from metals occur to the ligand (P−S) bonding orbitals rather than to (Nb−S) antibonding orbitals in the Nb_2PS_{10} part, which is supported by single-crystal X-ray data and the results of band-structure calculation. This work shows critical features that the solid-state ^{31}P NMR technique is a strong tool that can be used to investigate electron densities and chemical bonding natures around the P atoms in the quaternary metal thiophosphate family, especially in tetrahedral PS_4^{3-} systems.

Acknowledgment. This work was supported by the Korea Ministry of Science & Technology Foundation (99-N6-01) and by a grant (KRF-2000-015-DP0224) from the Korea Research Foundation. The Korea Basic Science Institute is acknowledged for the use of the Varian UnityInova200 and DSX400 solid-state NMR spectrometers.

CM010053V